ISSN 1062-8738, Bulletin of the Russian Academy of Sciences: Physics, 2024, Vol. 88, No. 4, pp. 523–530. © Pleiades Publishing, Ltd., 2024.

Modeling of Magnetic Hysteresis Parameters in Foraminiferal Shells of the Mid-Atlantic Ridge

E. S. Sergienko[a], S. Yu. Janson[a], K. G. Gareev[b, *], P. V. Kharitonskii[c], A. Yu. Ralin[d], T. S. Sheidaev[b], and E. A. Setrov[b]

[a] *St. Petersburg State University, St. Petersburg, 199034 Russia*
[b] *St. Petersburg Electrotechnical University "LETI," St. Petersburg, 197022 Russia*
[c] *Ioffe Institute, Russian Academy of Sciences, St. Petersburg, 194021 Russia*
[d] *Far Eastern Federal University, Vladivostok, 690922 Russia*
**e-mail: kggareev@etu.ru*

Received November 15, 2023; revised November 22, 2023; accepted December 28, 2023

Abstract—The composition and magnetic properties of foraminifers from bottom sediments of the Mid-Atlantic Ridge and their artificial analogs obtained by hydrothermal synthesis were studied. The presence of magnetic hysteresis and theoretical modeling of hysteresis characteristics made it possible to assume the presence of grains of nonstoichiometric magnetite in single- and few-domain states.

Keywords: foraminifera, hydrothermal synthesis, iron oxide, ferrimagnet, magnetic hysteresis, magnetic granulometry, theoretical modeling, magnetic state, magnetite

DOI: 10.1134/S1062873823706232

INTRODUCTION

One of the main tasks in the development of new functional materials containing magnetic nanoparticles is to obtain materials without toxic components and using "green" technologies [1]. Biogenic calcite skeletons have a number of advantages over artificially produced analogs, including better mechanical properties, biodegradability, biocompatibility, controllability of properties, and others [2, 3], which makes it urgent to study biomineralization processes on the skeletons of microorganisms and mollusks. Such objects are analogs of human bone material [4], and the introduction of various impurities containing metals into the calcite matrix significantly changes their properties and expands the scope of application. For example, it makes them suitable for use as pigments in paints, in targeted drug delivery [5], and tissue engineering [6]. Their increased porosity is also an important factor in optical applications [7].

Foraminifera shells are biogenic structures based on porous microparticles of calcium carbonate. Magnetic particles are formed in foraminifera during the processes of their mineral replacement [8]; in this case, calcium carbonate microparticles can be controlled by an external magnetic field. Also, magnetic structures on the skeleton of foraminifera can arise during the formation of iron-containing biogenic nodules on the surface of mineral skeletons [9]. To date, there have been few studies on foraminifera containing magnetic inclusions, which is why the magnetic properties of such objects have been poorly studied. In addition to the above, the study of the magnetic properties of objects of biogenic origin provides important information for solving problems of magnetic granulometry [10].

Carbonate remains of planktonic and benthic microorganisms are widespread in the Atlantic Ocean. Samples of Holocene and Upper Pleistocene sediments containing microbiota (mainly benthic and planktonic foraminifera and coccoliths) were collected on RV *Professor Logachev* during research by the Polar Marine Geological Exploration Expedition in the Russian exploration region of the Mid-Atlantic Ridge. This area is characterized by the widespread occurrence of relict and active hydrothermal structures. Under the influence of hydrothermal fluids, communities of microorganisms accumulate chemical elements in carbonate shells. Changes occur in the composition and structure of foraminiferal skeletons up to their complete replacement and disappearance [11, 12]. Planktonic foraminifera are subject to more intense changes due to the significantly greater porosity of their shells, greater sorption capacity, and higher solubility [13]. Many studies have shown that, under conditions of hydrothermal activity, foraminifera shells actively accumulate metals Fe, Cu, Co, Cr, Ni, and Ag. It was noted that, along the shells of microorganisms, iron oxyhydroxides develop, in particular goethite and ferromanganese formations, which form

Table 1. Description of the studied samples

Sample	Description
F_1	Powder of ground shells of the *Globorotalia* species
F_2	Powder of ground shells of the *Orbulina universa* species
F_{s1}	Single shell of the *Globorotalia menardi* species
F_{s2}	Single shell of the *Orbulina universa* species
F_{s3}	Single shell of the *Globigerinoides conglobatus* species
F_{art}	Powder of ground shells of the *Orbulina universa* species after hydrothermal deposition

small isometric accumulations on the surface of the shells [14].

The purpose of this work was to study the composition and magnetic properties of iron-containing formations located inside and on the surface of shells of the planktonic foraminifera species *Globigerinoides ruber*, *Globigerinoides conglobatus*, *Globigerinoides sacculifer*, *Globigerinoides tenellus*, *Orbulina universa*, *Globorotalia inflate*, *Globorotalia truncatulinoides*, and *Globorotalia menardii* from biogenic carbonate bottom sediments of hydrothermally active areas of the Mid-Atlantic Ridge. For comparative analysis, iron-containing formations on foraminifera *Orbulina universa* shells were synthesized, and their properties were studied. Hysteresis characteristics of the samples under study were also theoretically modeled.

EXPERIMENTAL

The petrographic structure and phase composition of the samples were identified by scanning electron microscopy (SEM) and energy-dispersive X-ray spectroscopy (EDX) using a QUANTA 200 3D DualBeam™ focused ion beam/scanning electron microscopes (FIB/SEM) system (FEI, Netherlands) with a Pegasus 4000 analytical complex (EDAX, United States) and a TM 3000 tabletop scanning electron microscope–microanalyzer (Hitachi, Japan). Magnetometric experiments consisted of measuring hysteresis loops in a maximum field of 7 T at 295 K and recording remanence decay curves in a 5-T field with a MPMS 3 magnetic property measurement system (Quantum Design, United States) in vibrating sample magnetometer mode with logarithmic field increment. The sensitivity of the magnetometer is 1×10^{-11} A m^2 in the absence of an external field, which makes it possible to measure weakly magnetic samples with the structure of a nonmagnetic matrix with a low content of ferrimagnetic impurities.

RESULTS AND DISCUSSION

Our previous work [15] considered the composition and magnetic properties of the foraminifera *Globigerinoides ruber* and *Globigerinoides sacculifer*, which look like black spherules with a shiny surface. Electron microscopic studies and EDX showed that the surface of the shells is composed of magnesium silicates—serpentine and talc, probably forming epimorphs. Analysis at a depth of 10 μm by ion etching showed the presence of calcium. This can be explained by the fact that the internal parts remained unreplaced. On the surface of the shells, skeletal aggregates of iron oxide crystallites were observed. According to morphological and magnetogranulometric data, these oxides are mainly represented by magnetite grains similar in size to single-domain grains.

Table 1 describes the samples studied in this work. Visually, foraminiferal shells with iron-containing formations can be divided into two types (Fig. 1):

(1) light-colored translucent shells through the thin surface of which one can see dark-colored crusts lining completely or partially the inner surface (samples F_1 and F_2);

(2) light-colored shells on the surface of which microcrystalline (and possibly amorphous) mineral aggregates grow in the form of crusts and clusters of black color (samples F_{s1}, F_{s2}, and F_{s3}).

According to EDX data (Table 2), the foraminifera shells have a predominantly carbonate (calcite) composition. They can be either unchanged, well preserved, or affected by recrystallization processes with enlargement of calcite grains, or replacement by opal. Crusts and growths are observed on both the outer and inner surfaces of shells. The internal crusts of shells of the first type consist of iron oxides (hydroxides), while growths and crusts on shells of the second type show the presence of iron and manganese in their composition. These are probably cryptocrystalline aggregates of oxides and hydroxides of iron and manganese. Along with oxides, pyrite is also found in the form of separate aggregates, sometimes framboids.

In addition, for the purpose of comparative analysis, sample F_{art} was synthesized; it was a powder of ground shells of the species *Orbulina universa*, which initially did not contain noticeable internal and external dark inclusions. An attempt was made to experimentally reproduce the conditions for the formation of iron-containing phases on foraminifera shells [16–19]. For this purpose, hydrothermal synthesis of iron oxide nanoparticles was carried out in an aqueous sus-

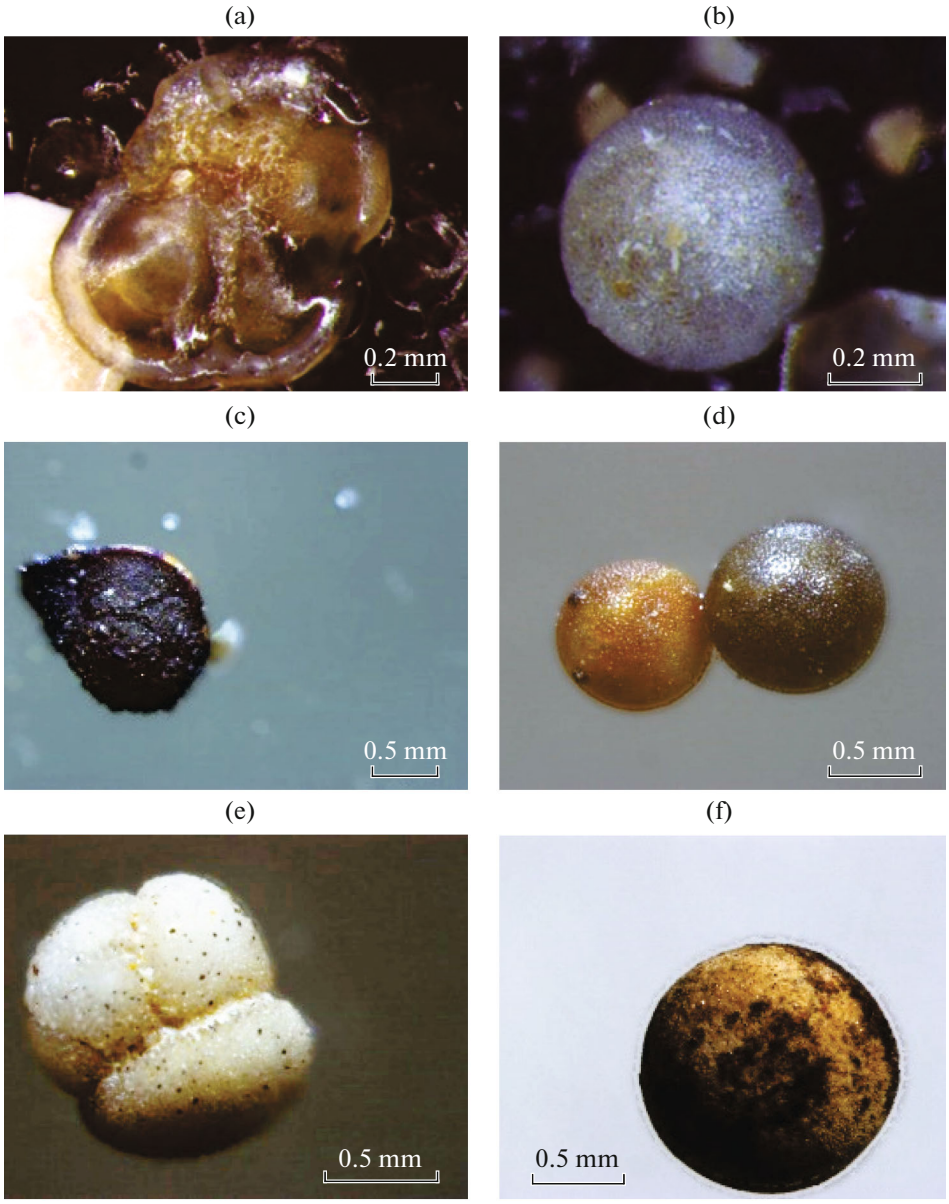

Fig. 1. Optical images of foraminifera samples: (a) F_1, *Globorotalia menardii*; (b) F_2, *Orbulina universa*; (c) F_{s1}, *Globorotalia menardii*; (d) F_{s2}, *Orbulina universa*; (e) F_{s3}, *Globigerinoides conglobatus*; and (f) F_{art}, *Orbulina universa*.

pension of foraminifera: a sample of "pure" unsubstituted calcite shells weighing 100 mg was added to 14 mL of distilled water with continuous stirring. Then, 0.001 mol of $FeSO_4 \cdot 7H_2O$ (pure grade, Len-Reaktiv, Russia) and 0.002 mol of $Fe(NO_3)_3 \cdot 9H_2O$ (reagent grade, ReaktivTorg, Russia) were dissolved in the obtained suspension. After this, iron(II) and (III) hydroxides were coprecipitated with a 25% ammonia solution until a dark green precipitate formed (pH 12). The resulting reaction mixture was transferred to a Teflon cell of a 15-mL steel autoclave. The autoclave was hermetically sealed, and its contents were kept isothermally at 180°C and a pressure of 100 MPa for 4 h. Next, foraminifera with iron oxide nanoparticles on the surface were removed from the autoclave, washed several times with distilled water, and dried at 60°C to constant weight.

To more accurately identify iron minerals, in this work, the magnetic properties of iron-containing shells were studied. Figure 2 shows the hysteresis loops of the samples on which the saturation magnetization M_s, saturation remanence M_{rs}, coercivity H_c, and remanence coercivity H_{cr} were measured. The measurements were carried out both on single shells and on powders of ground shells of foraminifera of the same type of replacement. In the former case, the measured values of the magnetic moment could be close to the sensitivity limit of the magnetometer (10^{-9}–10^{-10} A m^2).

Table 2. Contents of chemical elements in iron-containing formations of samples of various types according to EDX data, wt % (excluding carbon)

Element	F_1	F_{s2}	F_{art}
O	36.32	30.57	30.83
Mg	2.96	3.07	–
Al	3.97	3.74	1.17
Si	3.88	5.01	1.69
P	–	1.77	5.57
S	–	–	0.79
K	0.39	–	–
Ca	13.22	10.11	20.57
Ti	0.47	–	–
Mn	–	19.12	–
Fe	38.79	26.61	39.38

Table 3. Parameters of magnetic hysteresis of foraminifera samples

Sample	m, mg	$\mu_0 H_c$, mT	$\mu_0 H_{cr}$, mT	M_s, A m^2/kg	M_{rs}, A m^2/kg	H_{cr}/H_c	M_{rs}/M_s
F_1	10.59	4.7	25.0	0.010	0.0006	5.3	0.060
F_2	10.63	6.0	35.0	0.043	0.0014	5.8	0.033
F_{s1}	0.10	9.0	30.0	0.027	0.0040	3.3	0.148
F_{s2}	0.10	7.0	20.0	0.090	0.0040	2.9	0.044
F_{s3}	0.08	1.0	32.0	0.033	0.0032	2.0	0.097
F_{art}	2.89	0.15	7.0	1.700	0.0120	46.7	0.007

Table 3 shows the weights and magnetic hysteresis parameters of the samples under study. According to magnetic granulometry data [10], the values of the M_{rs}/M_s and H_{cr}/H_c ratios for all foraminiferal samples indicate that they contain a significant amount of fairly large single- and few-domain (pseudo-single-domain) particles, and the artificial sample F_{art} should contain a large number of smaller (superparamagnetic) particles.

Under the approximation of a log–normal volume distribution of particles [20, 21], it is possible to calculate the most probable characteristic sizes of particles in various magnetic states [22]. The probability density of the log–normal distribution is written as

$$\varphi(x) = \frac{1}{x\sigma\sqrt{2}}\exp\left(-\frac{\left(\ln(x/\alpha)\right)^2}{2\sigma^2}\right), \qquad (1)$$

where $x = v/v_p$ is the ratio of the particle volume to the mean volume, σ is the standard deviation, and α is the mean value of the corresponding Gaussian distribution.

In modeling, four ranges of grain sizes corresponding to different magnetic states were considered: superparamagnetic (SP), single-domain (SD), pseudo-single-domain (PSD), and multidomain (MD) particles with sizes of 0–25, 25–40, 40–100, and 100–500 nm, respectively (see, e.g., [23–26]). By PSD particles, we mean particles with vortex structures and a small number of domains, and the contribution of multidomain particles to the hysteresis characteristics are neglected.

Let us introduce the relative numbers of particles corresponding to the above magnetic states: n_{sp}, n_{sd}, n_{psd}, and n_{md}. The relative number of particles of each group is expressed as

$$n = \int_{x_1}^{x_2} \varphi(x)\,dx \Big/ \int_{x_{min}}^{x_{max}} \varphi(x)\,dx, \qquad (2)$$

where x_1 and x_2 are the lower and upper limits of the volume range of a given group of particles, respectively; and x_{min} ($d = 0$) and x_{max} ($d = 500$ nm) are the minimum and maximum relative volumes of particles, respectively, and $x_2 \le x_{max}$.

In our previous work [22], it was taken into account that the samples contain SP particles blocked by magnetostatic interaction, which can contribute not only to the saturation magnetization, but also to the saturation remanence of the sample. Therefore, two groups of SP particles can be distinguished: nbSP particles,

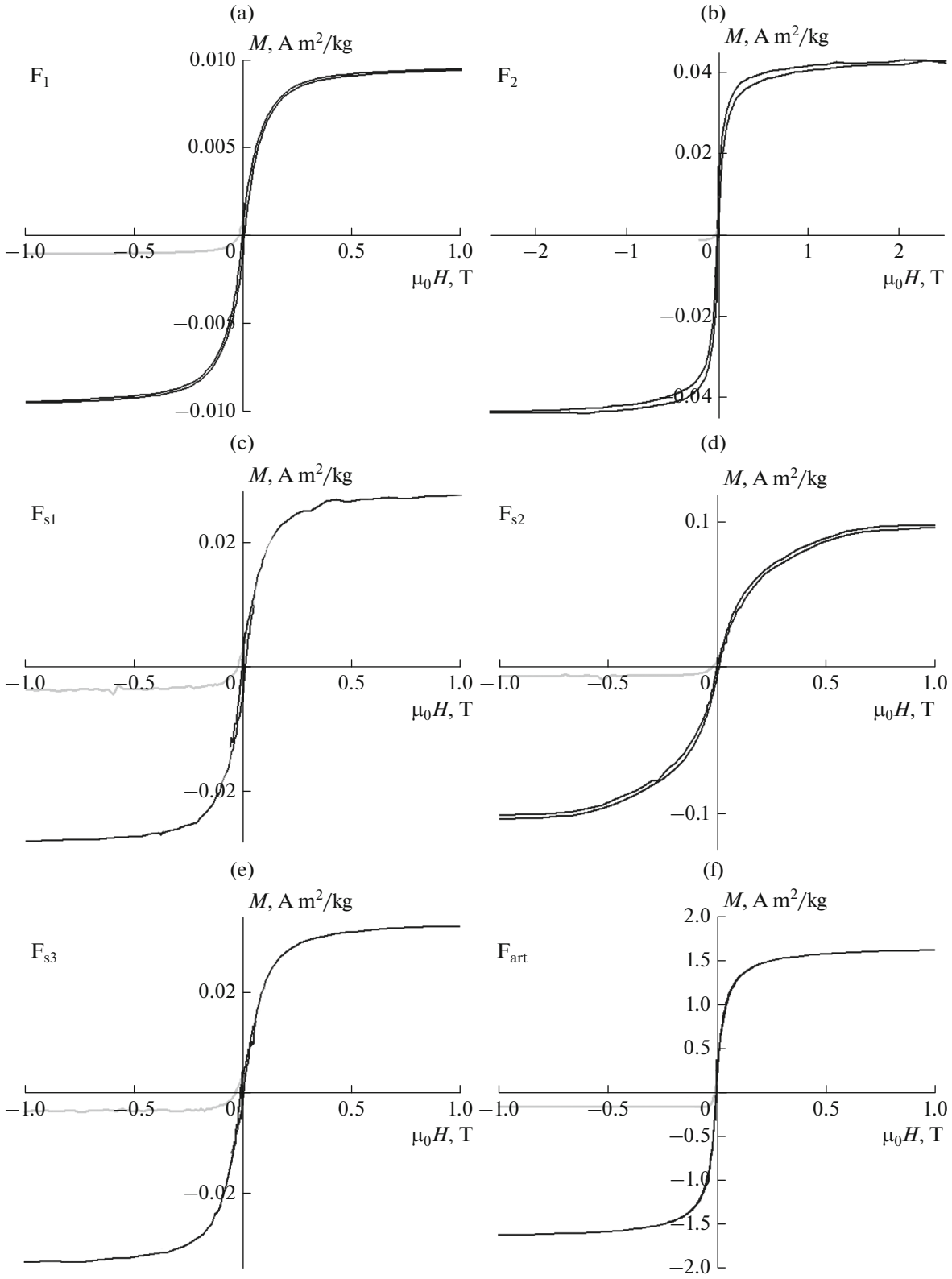

Fig. 2. Hysteresis loops in a field less than 1 T and reverse field demagnetization curves for samples (a) F_1, (b) F_2, (c) F_{s1}, (d) F_{s2}, (e) F_{s3}, and (f) F_{art}. The saturation magnetization values obtained in a field of 7 T are given in Table 3.

Table 4. Fractions of the volume concentration of ferrimagnetic particles in the corresponding magnetic states, d_{mean} is the mean size of ferrimagnetic particles in the sample

nbSP, %	C_{nbsp}	C_{bsp}	C_{sd}	C_{psd}	C_{md}	d_{mean}, nm
1	0.01	0.04	0.11	0.46	0.38	36
10	0.10	0.24	0.31	0.35	0.00	19
25	0.25	0.20	0.22	0.33	0.00	7

which are unblocked (true) superparamagnetic particles (0–15 nm); and bSP particles, which are blocked superparamagnetic particles (15–25 nm) (see, e.g., [27]).

For further modeling, three particle size distributions were chosen (Table 4), the first of which was used for samples with a low content of nbSP particles (about 1%); and the other two, for sample F_{art}, which, according to magnetic granulometry, clearly contains a significantly larger number of nbSP particles.

The relative number of nbSP particles is found according to formula (2) at $x_1 = 0$ and $x_2 = x_{bsp}$ (the volume corresponding to the blocking size, in our case, $d_{bsp} = 15$ nm). Then the relative mean volume of nbSP particles is

$$x_{nbsp} = \int_0^{x_{bsp}} x\varphi(x)\,dx. \quad (3)$$

Similarly, one can calculate the relative mean volumes of the other particles in different magnetic states. In this case, the mean volume and mean size of ferrimagnetic particles in the sample can be calculated using the formulas

$$v_{mean} = v_p(n_{nbsp}x_{nbsp} + n_{bsp}x_{bsp} + n_{sd}x_{sd} + n_{psd}x_{psd} + n_{md}x_{md}), \quad d_{mean} = (6v_{mean}/\pi)^{1/3}. \quad (4)$$

Then the fraction of the volume concentration of unblocked ferrimagnetic particles in the sample is

$$C_{nbsp} = n_{nbsp}\frac{V_{nbsp}}{V_{mean}}, \quad \text{where} \quad v_{nbsp} = v_p x_{nbsp}. \quad (5)$$

The best results for various C_{nbsp} (consistent with experimental values of M_{rs}, M_s, H_{cr}, H_c) were obtained using the characteristic sizes of ferrimagnetic particles $d_p = 40$ nm (foraminiferal samples) and 15 nm (sample F_{art}) and the corresponding volumes of a spherical particle $v_p = (\pi/6)d_p^3$.

Further calculations were made using the model of single-domain particles with effective spontaneous magnetization (SDEM model), which takes into account the magnetostatic interaction between ferrimagnetic particles [28–30].

Using the SDEM model, in the mean field approximation, it is possible to take into account the influence of magnetostatic interaction and to obtain distribution functions of random fields at any volume concentrations of a ferrimagnet [31]. Further, using the experimental values of magnetization M_s, saturation remanence M_{rs}, coercivity H_c, and remanence coercivity H_{cr}, one can calculate the effective spontaneous magnetization of particles: by saturation magnetization, $I_{s\,eff}$; and by saturation remanence, $I_{rs\,eff}$. The introduction of effective spontaneous magnetizations makes it possible to evaluate the effect of the inhomogeneity of the magnetic moment in the bulk of the particle, which is determined by the formation of domain and vortex structures, as well as possible chemical inhomogeneity [32–34].

The magnetizations $I_{s\,eff}$ and $I_{rs\,eff}$ were found by solving the inverse problem of matching the theoretical values of these magnetizations, calculated using both models, with experimental data. The calculations were performed using dimensionless magnetization ζ and volume concentration C_f of ferrimagnetic particles involved in its formation:

$$\zeta = \frac{M}{C_f I_{eff}}, \quad C_f = N\frac{V_{mean}}{V_s}. \quad (6)$$

Here, M means M_s or M_{rs}, and N is the number of particles with mean volume v_{mean} and concentration C_f in a sample of volume V_s. The magnetization of a system of uniaxial ferrimagnetic particles randomly distributed in a cylindrical volume is determined using the modified method of moments and the expansion in the Gram–Charlier series [31, 35].

As mentioned above, the interaction leads to blocking of the magnetic moments of some SP particles, which contribute to the saturation remanence [35]. Then the experimental values of M_s and M_{rs} agree with the results of calculations using the SDEM model:

$$M_s = C_f I_{s\,eff}, \quad M_{rs} = C_f(1 - C_{nbsp} - C_{md})I_{rs\,eff}. \quad (7)$$

In modeling, the spontaneous magnetization of magnetite, taking into account possible nonstoichiometry, was taken to be $I_s = 450 \times 10^3$ A/m [36]. The results are shown in Table 5.

For foraminifera samples, the best agreement with experimental data is obtained when the content of true superparamagnetic particles (nbSP) in the ferrimagnetic fraction is no more than 1%. At the same time, the volume concentration of the ferrimagnet (nonstoichiometric magnetite) in the samples is low and is in

Table 5. Volume concentrations C_f of the ferrimagnet in samples and the corresponding effective spontaneous magnetizations $I_{rs\ eff}$ based on saturation remanence. For all samples, the effective spontaneous saturation magnetization is $I_{s\ eff} = 450 \times 10^3$ A/m

Sample	nbSP, %	C_f, 10^{-3}	$I_{rs\ eff}$, kA/m
F_1	1	0.01	236
F_2	1	0.05	140
F_{s1}	1	0.03	365
F_{s2}	1	0.11	94
F_{s3}	1	0.02	146
F_{art}	10	1.74	168
	25	1.74	201

the range of 10^{-5}–10^{-4}, and the effective spontaneous magnetization $I_{rs\ eff}$ is about 100–350 kA/m. Judging by the mean grain size (36 nm) and the $I_{rs\ eff}$ value, it can be assumed that the magnetic properties of foraminiferal samples are mainly determined by single- and few-domain particles similar in composition to magnetite.

The ferrimagnetic fraction of artificial sample F_{art} obtained by hydrothermal synthesis of magnetite grains on foraminiferal skeletons contains a large fraction of nbSP particles. Taking into account the magnetogranulometric ratios (see Table 3), the modeling was carried out for fractions of 10 and 25% and mean grain sizes of 19 and 7 nm, respectively. At much higher ferrimagnetic concentration (about 10^{-3}), the effective spontaneous magnetization $I_{rs\ eff}$ is of the same order of magnitude as that for foraminiferal samples.

Since all the studied foraminiferal samples contained internal dark films, it can be assumed that the magnetite in them is of biogenic origin; the mean grain size is close to the single-domain limit of the order of 40 nm [10]. For the artificial sample, the foraminiferal skeletons do not contain internal dark films, and the magnetite particles synthesized on the surface have a wider size spread, including a significant amount of superparamagnetic particles.

CONCLUSIONS

The study was mase of the composition and magnetic properties of iron-containing formations located inside and on the surface of foraminiferal shells from biogenic carbonate bottom sediments of hydrothermally active areas of the Mid-Atlantic Ridge, as well as artificial formations obtained by hydrothermal synthesis.

Two types of foraminiferal shells were studied: shells predominantly containing internal dark-colored crusts, and shells containing external microcrystalline crusts and black clusters. In addition to the significant content of carbon, oxygen, calcium, and iron in the growths, shells of the second type also contain large amounts of manganese.

The measured parameters of magnetic hysteresis confirmed the presence of a noticeable ferrimagnetic component and, according to magnetic granulometry data, suggest that foraminiferal samples are dominated by single- and few-domain particles; and artificial samples, by smaller superparamagnetic particles.

The theoretical modeling of the hysteresis characteristics of the samples under study made it possible to estimate the composition and volumetric concentrations of the ferrimagnet (nonstoichiometric magnetite), which makes the main contribution to the saturation remanence. At the same time, the volume concentration of the ferrimagnet in the samples is low (10^{-5}–10^{-4}), and the effective spontaneous magnetization is about 100–350 kA/m, which is significantly higher than that of iron hydroxides, but lower than that of pure magnetite. Most likely, this is explained by the chemical and magnetic heterogeneity of the grains, the mean size of which is about 40 nm.

The ferrimagnetic fraction of artificial samples contains a large fraction of superparamagnetic particles. The modeling showed that the effective spontaneous magnetization is of the same order of magnitude as for foraminiferal samples, but the ferrimagnetic concentration is significantly higher and the mean grain size is smaller (about 10–20 nm).

ACKNOWLEDGMENTS

We are grateful to I.G. Dobretsova, mineralogist, OOO PMGE, for providing samples for the study; and A.N. Bugrov, Associate Professor, Department of Physical Chemistry, St. Petersburg Electrotechnical University "LETI," for carrying out hydrothermal treatment of foraminifera shells.

The study was carried out using the equipment of the Resource Centers of the Research Park of the St. Petersburg State University: "Center for Diagnostics of Functional Materials for Medicine, Pharmacology, and Nanoelectronics"; "Geomodel"; "Resource Center for Microscopy and Microanalysis"; "X-ray diffraction research methods"; and "Center for Innovative Technologies of Composite Nanomaterials."

FUNDING

This work was supported by ongoing institutional funding. No additional grants to carry out or direct this particular research were obtained.

ETHICS APPROVAL AND CONSENT TO PARTICIPATE

This work does not contain any studies involving human and animal subjects.

CONFLICT OF INTEREST

The authors of this work declare that they have no conflicts of interest.

REFERENCES

1. Maliszewska, I., Kocek, D., and Wanarska, E., *Physicochem. Probl. Miner. Process.*, 2020, vol. 56, no. 6, p. 244.
2. Shi, R.J., Lang, J.Q., Wang, T., Zhou, N., and Ma, M.G., *Front. Bioeng. Biotechnol.*, 2022, no. 10, p. 937266.
3. Magnabosco, G., Hauzer, H., Fermani, S., et al., *Mater. Horiz.*, 2019, no. 6, p. 1862.
4. Takano, H., Manabe, E., Hirano, M., and Okazaki, M., *Appl. Biochem. Biotechnol.*, no. 40, p. 239.
5. Moheimani, N.R., Web, J.P., and Borowitzka, M.A., *Algal Res.*, 2012, no. 1, p. 120.
6. Titelboim, D., Sadekov, A., Blumenfeld, M., et al., *Ecol. Indic.*, 2021, vol. 120, p. 106931.
7. Dorozhkin, S.V., *Biomatter*, 2011, no. 1, p. 3.
8. Pawlowski, J. and Majewski, W., *J. Foraminifer Res.*, 2011, vol. 41, no. 1, p. 3.
9. Yang, H., Peng, X., Gooday, A.J., et al., *Geochem. Persp. Lett.*, 2022, no. 21, p. 23.
10. Kirshvink, J.L., *Magnetite Biomineralization and Magnetoreception in Organisms: A New Biomagnetism*, New York: Plenum, 1985.
11. Gablina, I.F., Demina, L.L., Dmitrenko, O.B., et al., *Okeanology*, 2011, vol. 51, no. 3, p. 476.
12. Gablina, I.F., Dmitrenko, O.B., Khusid, T.A., and Libina, N.V., *Lithol. Miner. Resour.*, 2019, vol. 54, no. 6, p. 511.
13. Khusid, T.A., Os'kina, N.S., Lukashina, N.P., et al., *Stratigr. Geol. Correl.*, 2018, vol. 26, no. 1, p. 109.
14. Gablina, I.F., Dobretsova, I.G., Popova, E.A., et al., *Lithol. Miner. Resour.*, 2021, vol. 56, no. 2, p. 113.
15. Sergienko, E., Janson, S., Kharitonskii, P., et al., in *Biogenic–Abiogenic Interactions in Natural and Anthropogenic Systems*, Cham: Springer, 2023, p. 153.
16. Pierre, S., Gysi, A.P., and Monecke, T., *Geofluids*, 2018, vol. 2018, p. 1389379.
17. Kennedy, C.B., Scott, S.D., and Ferris, F.G., *Geomicrobiol. J.*, 2003, vol. 20, no. 3, p. 199.
18. Ding, K., Seyfried, W.E., Jr., Zhang, Z., et al., *Earth Planet. Sci. Lett.*, 2005, vol. 237, nos. 1–2, p. 167.
19. Agarwal, D.K. and Palayil, J.K., *Sci. Rep.*, 2022, vol. 12, no. 1, p. 6811.
20. Olin, M., Anttila, T., and Dal Maso, M., *Chem. Phys.*, 2016, vol. 16, p. 7067.
21. Fujihara, A., Tanimoto, S., Yamamoto, H., and Ohtsuki, T., *J. Phys. Soc. Jpn.*, 2018, vol. 87, p. 034001.
22. Kharitonskii, P., Bobrov, N., Gareev, K., et al., *J. Magn. Magn. Mater.*, 2022, vol. 553, p. 169279.
23. Dunlop, D.J., *J. Geophys. Res.*, 1973, vol. 78, p. 1780.
24. Butler, R.F. and Banerjee, S., *J. Geophys. Res.*, 1975, vol. 80, p. 4049.
25. Banerjee, S., *IEEE Trans. Magn.*, 1979, vol. 15, no. 5, p. 1241.
26. Nagy, L., Williams, W., Tauxe, L., and Muxworthy, A.R., *Geochem., Geophys., Geosyst.*, 2019, vol. 20, no. 6, p. 2907.
27. Kharitonskii, P.V., Gareev, K.G., Ionin, S.A., et al., *J. Magn.*, 2015, vol. 20, p. 221.
28. Kharitonskii, P.V., *Fiz. Tverd. Tela*, 1997, vol. 39, no. 1, p. 185.
29. Kharitonskii, P., Kirillova, S., Gareev, K., et al., *IEEE Trans. Magn.*, 2020, vol. 56, p. 7200209.
30. Kharitonskii, P.V., Kosterov, A.A., Gurylev, A.K., et al., *Phys. Solid State*, 2020, vol. 62, p. 1691.
31. Al'miev, A.S., Ralin, A.Yu., and Kharitonskii, P.V., *Fiz. Met. Metalloved.*, 1994, vol. 78, no. 1, p. 28.
32. Roberts, A.P., Almeida, T.P., Church, N.S., et al., *J. Geophys. Res.: Solid Earth*, 2017, vol. 122, p. 9534.
33. Starowicz, M., Starowicz, P., Zukrowski, J., et al., *J. Nanopart. Res.*, 2011, vol. 13, p. 7167.
34. Roberts, A.P., Tauxe, L., Heslop, D., et al., *J. Geophys. Res.: Solid Earth*, 2018, vol. 123, p. 2618.
35. Kharitonskii, P., Zolotov, N., Kirillova, S., et al., *Chin. J. Phys.*, 2022, vol. 78, p. 271.
36. Dunlop, D.J. and Özdemir Ö., *Rock Magnetism: Fundamentals and Frontiers*, Cambidge: Cambridge Univ. Press, 1997.